Electronic Supplementary Material (ESI) for Chemical Science.

Free-standing 2D non-van der Waals antiferromagnetic hexagonal FeSe semiconductor: halide-assisted chemical synthesis and Fe^{2+} related magnetic transitions

Junjie Xu,[a] Wei Li,[a] Biao Zhang,[a] Liang Zha,[b] Wei Hao,[c] Shixin Hu,[d] Jinbo Yang,[b] ShuZhou Li,[c] Song Gao,[e,f] and Yanglong Hou*[a]

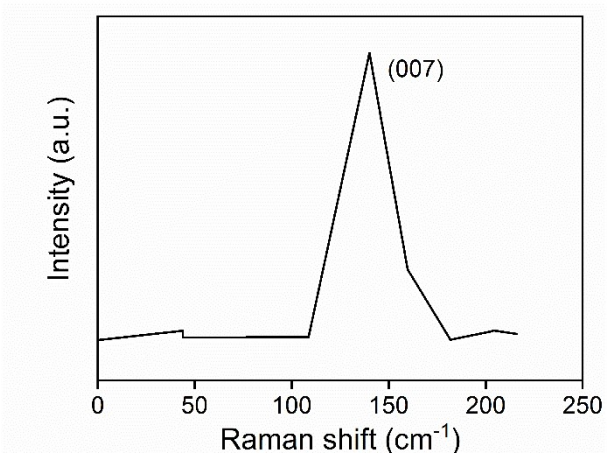

Fig. S1 The first-principles Raman investigation of hexagonal FeSe with five-unit-cell thickness.

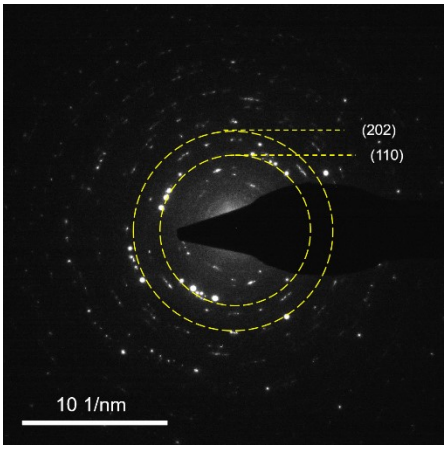

Fig. S2 The SAED patterns of hexagonal FeSe nanosheets.

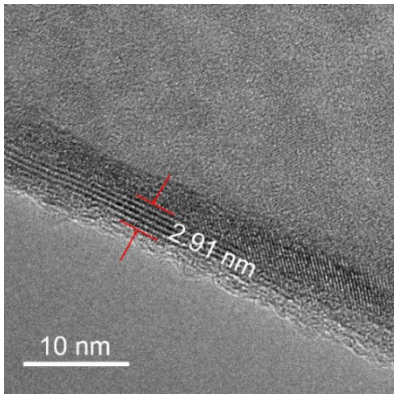

Fig. S3 HRTEM image of the rolled-up edge of 2D hexagonal FeSe.

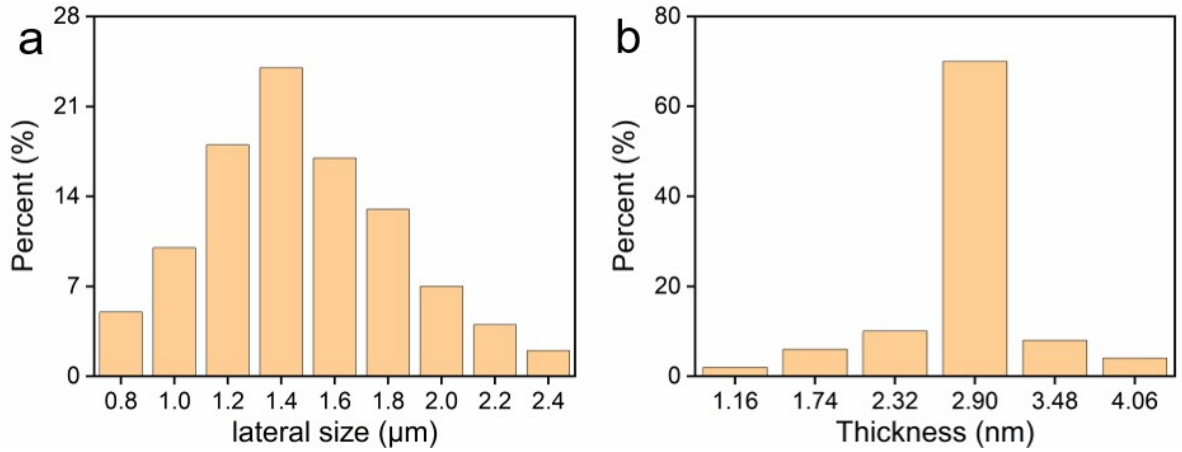

Fig. S4 (a) lateral size and (b) thickness distribution of 2D hexagonal FeSe.

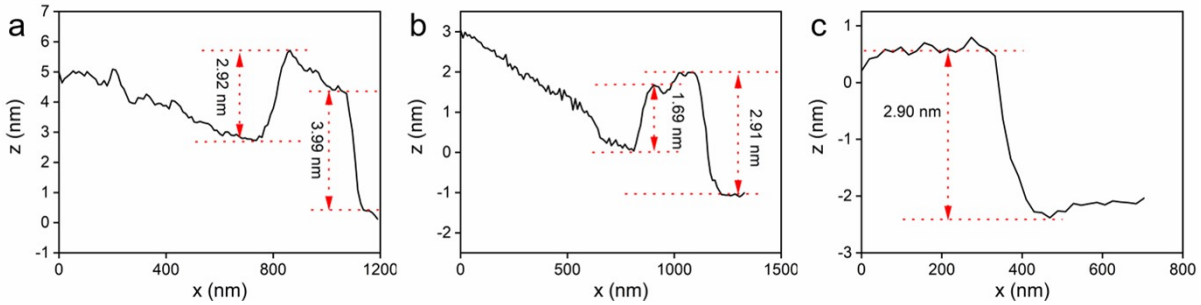

Fig. S5 Line profile scan of hexagonal FeSe nanosheets.

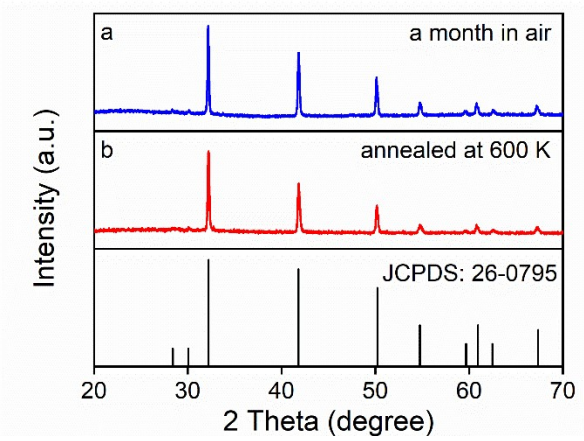

Fig. S6 XRD patterns of the 2D hexagonal FeSe (a) exposed to air for a month and (b) heat-treated at 600K under the N_2 atmosphere for 1 h.

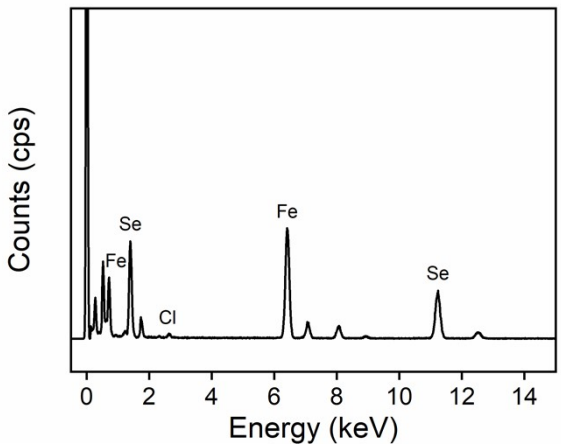

Fig. S7 EDX Spectra of the 2D hexagonal FeSe.

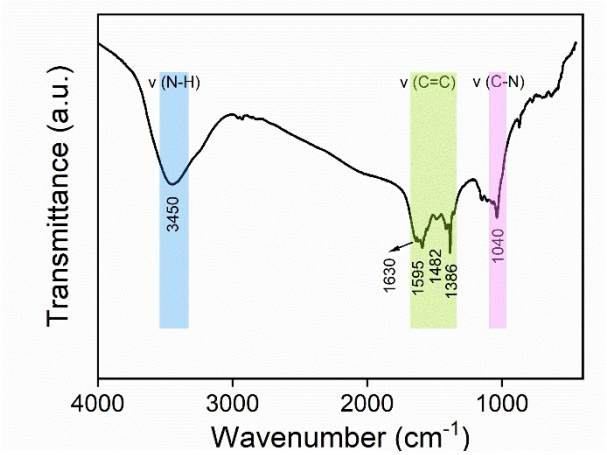

Fig. S8 FT-IR spectroscopy of the 2D hexagonal FeSe.

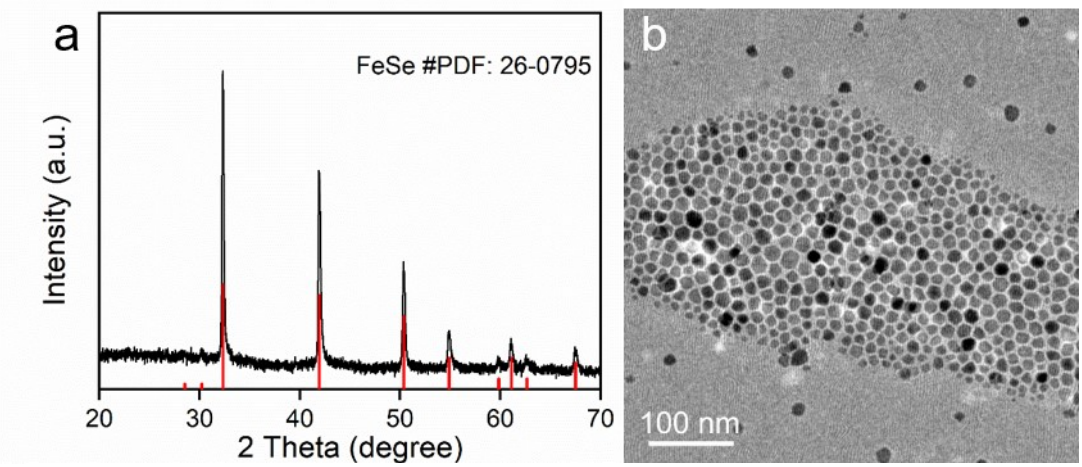

Fig. S9 (a) XRD pattern and (b) TEM image of hexagonal FeSe nanoparticles obtained by the reaction between ODE-Se complex and $Fe(acac)_2$.

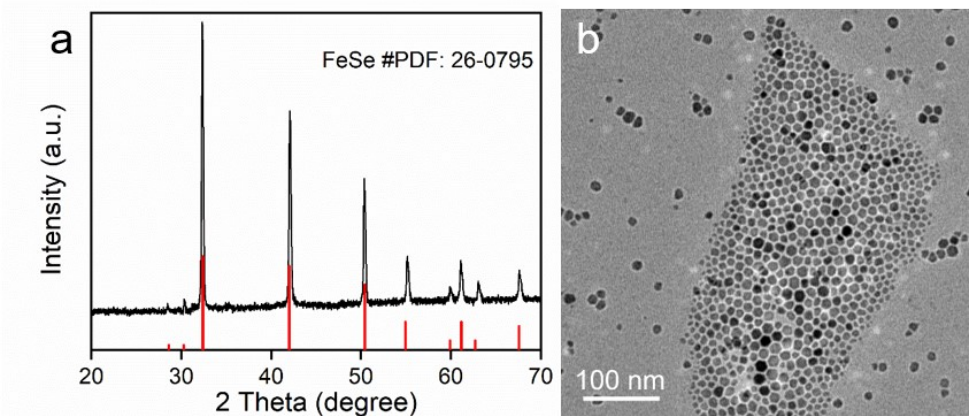

Fig. S10 (a) XRD pattern and (b) TEM image of hexagonal FeSe nanoparticles obtained by the reaction between ODE-Se complex and $Fe(acac)_2$ with the presence of Cl^-.

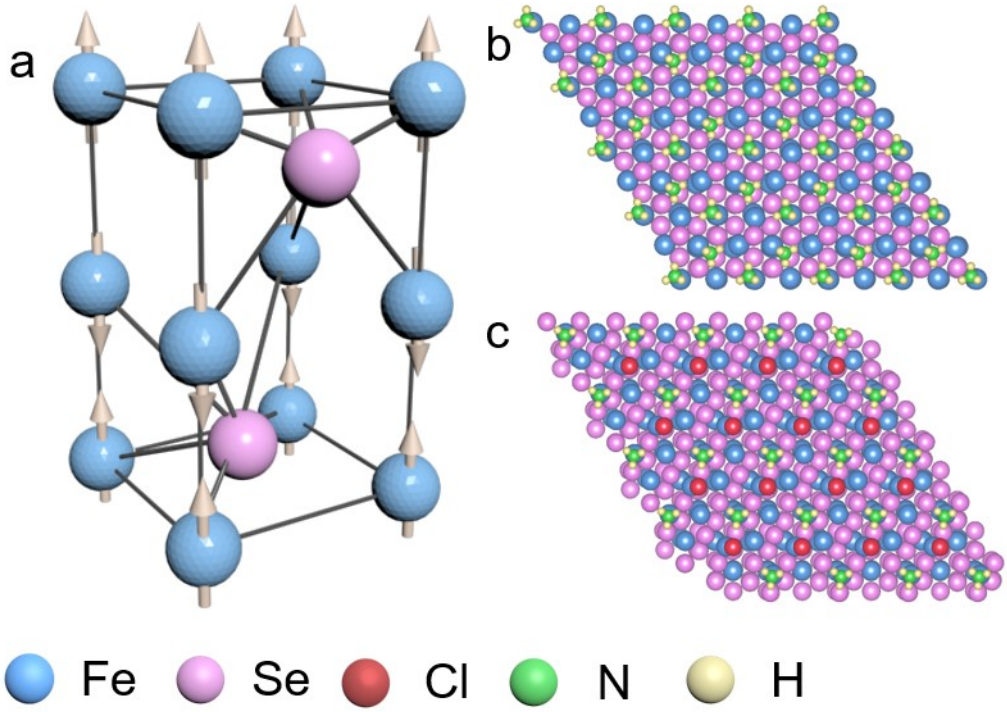

Fig. S11 (a) Crystal structure of hexagonal FeSe. The upward and downward arrows represnet spin-up and spin-down states, respectively. Calculation model of (b) NH_3, as well as (c) NH_3 and Cl^- adsorption on (001) facet.

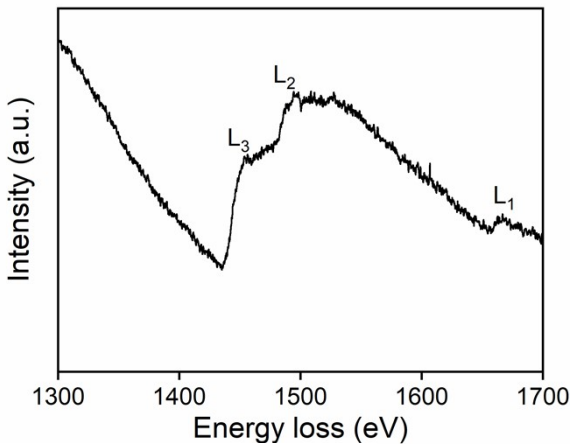

Fig. S12 Se L-edge EELS of 2D ultrathin hexagonal FeSe.

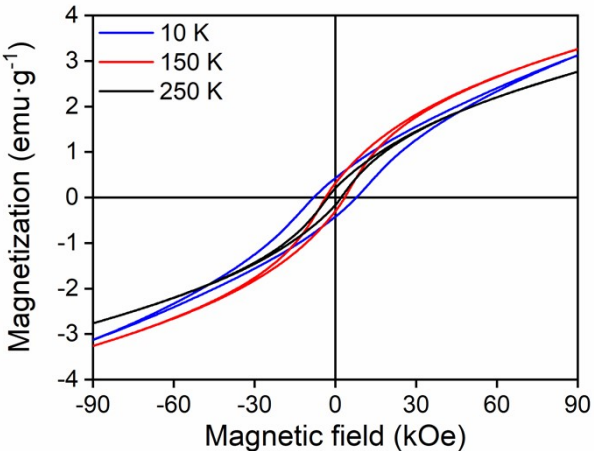

Fig. S13 Hysteresis loops of 2D ultrathin hexagonal FeSe between 10 and 250 K.

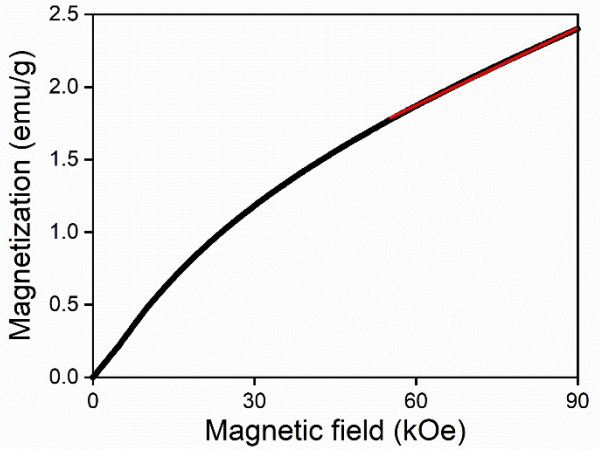

Fig. S14 Initial magnetization curve of 2D ultrathin hexagonal FeSe at 300 K.

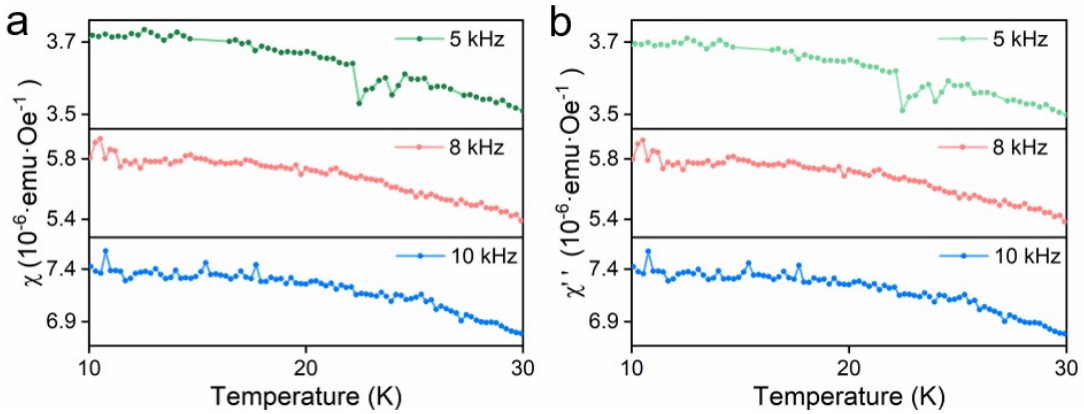

Fig. S15 Temperature dependence of (a) ac susceptibility, χ, and (b) out-of-plane component, χ'', of 2D ultrathin hexagonal FeSe at different frequencies.

Table S1 Isomer shift, quadrupolar splitting, and magnetic field of as-synthesized hexagonal FeSe nanosheets

Temperature	Fe site	Area (%)	Amplitude/ Standard deviation	Isomer shift ($mm \cdot s^{-1}$)	Quadrupolar splitting ($mm \cdot s^{-1}$)	Magnetic field (T)
300 K	1	28.12	3834.21/258	0.601	-0.151	22.290
	2	26.98	3909.35/258	0.852	0.282	22.125
	3	44.90	35756.52/531	0.351	0.763	0
30 K	1	16.83	1371.29/130	0.229	-0.181	42.162
	2	10.65	867.99/165	0.753	0.136	42.699
	3	44.49	3625.78/120	0.860	-0.204	28.689
	4	22.52	1835.55/237	0.844	-0.286	24.447
	5	5.51	2693.55/453	0.750	1.292	0
10 K	1	8.24	1426.08/140	0.202	-0.204	49.535
	2	23.85	2007.22/96.1	0.535	0.084	49.568
	3	9.84	847.78/89.5	0.878	-0.832	45.041
	4	32.29	2956.79/143	0.860	-0.232	28.486
	5	25.78	2031.25/126	0.773	-0.391	25.163

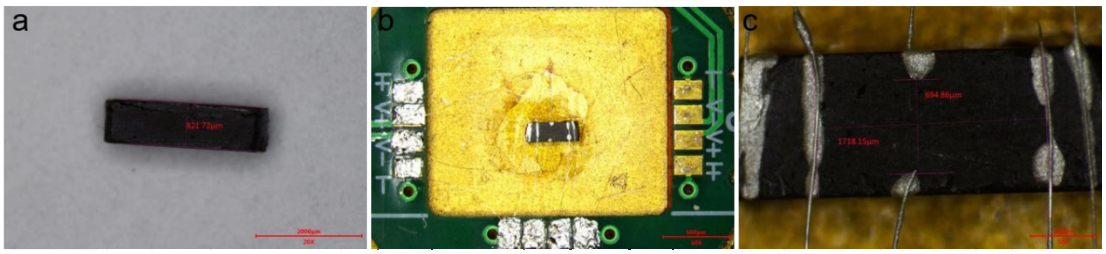

Fig. S16 (a) The thickness of the pellet. (b) and (c) pressed pellets device of as-synthesized FeSe nanosheets for variable-temperature conductivity measurements by *van der Pauw* method with different magnifications.

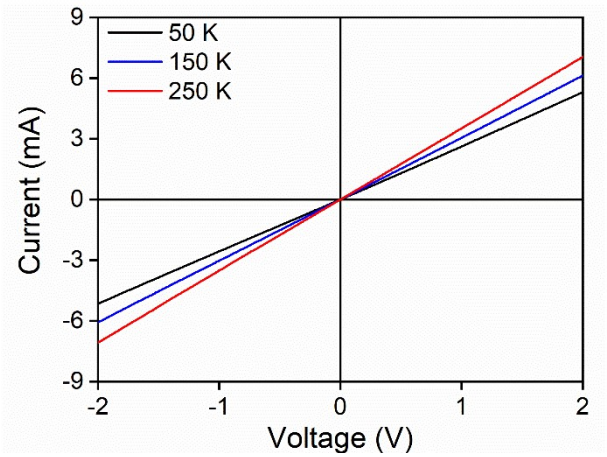

Fig. S17 I-V curves of 2D ultrathin hexagonal FeSe at different temperatures.

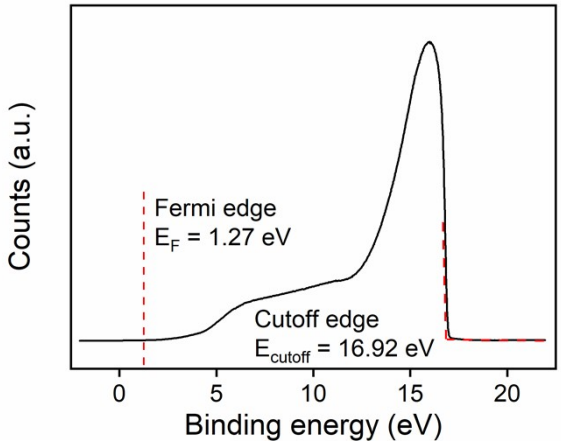

Fig. S18 UPS spectra of 2D hexagonal FeSe.